Cavity Length Effects on Internal Loss and Quantum Efficiency of Multiquantum-Well Lasers

Joachim Piprek, *Senior Member, IEEE*, Patrick Abraham, and John E. Bowers, *Fellow, IEEE*

***Abstract*— We investigate loss mechanisms in 1.55-μm InGaAsP–InP multiquantum-well ridge-waveguide laser diodes at room temperature. The common method of measuring light versus current curves and plotting the inverse slope efficiency versus laser length is employed to extract the internal optical loss α_i and the differential internal efficiency η_i. This method neglects the dependence of both the parameters on the laser cavity length L. We analyze physical mechanisms behind these loss parameters and their length dependence using the commercial laser simulation software PICS3D. Internal optical losses are dominated by carrier density dependent absorption. The differential internal efficiency above threshold is found to be mainly restricted by carrier recombination losses within the quantum wells, i.e., Fermi level pinning is not observed. Both loss mechanisms are enhanced with shorter cavity length due to the higher quantum well carrier density. For the shortest device measured ($L = 269$ μm), we extract $\alpha_i = 20$ cm^{-1} and $\eta_i = 66\%$. With increasing cavity length, the loss parameters approach $\alpha_i = 15$ cm^{-1} and $\eta_i = 70\%$. From the inverse slope efficiency versus cavity length plot, we obtain $\alpha_i = 14$ cm^{-1} and $\eta_i = 67\%$ independent of laser length.**

***Index Terms*— Error analysis, laser measurements, numerical analysis, optical losses, quantum-well devices, semiconductor device modeling, semiconductor lasers, simulation software.**

I. Introduction

THE DIFFERENTIAL quantum efficiency η_d is one of the key performance parameters of laser diodes. It can be obtained from the slope of the light output power versus current (L–I) characteristic above threshold. This efficiency $\eta_d = \eta_i \eta_o$ depends on carrier losses (η_i) and photon losses (η_o). The later can be expressed as $\eta_o = \alpha_m/(\alpha_i + \alpha_m)$ using the internal optical loss coefficient α_i and the optical mirror loss coefficient α_m. In a symmetric Fabry–Perot cavity, both the mirror losses are identical and $\alpha_m = L^{-1} \ln(1/R)$ depends on laser length L and facet power reflectivity R, which leads to the common expression

$$\frac{1}{\eta_d} = \frac{1}{\eta_i}\left(\frac{L\alpha_i}{\ln R^{-1}} + 1\right). \tag{1}$$

Manuscript received December 1, 1998; revised April 5, 1999.

This work was supported by the Center for Multidisciplinary Optical Switching Technology (MOST), a DARPA-sponsored Multidisciplinary Research Initiative (MURI).

The authors are with the Department of Electrical and Computer Engineering, University of California at Santa Barbara, Santa Barbara, CA 93106 USA.

Publisher Item Identifier S 1077-260X(99)06946-4.

This equation gives a linear dependence $\eta_d^{-1}(L)$ and it is widely used to determine the loss parameters η_i and α_i from L–I measurements with different laser lengths [1]. This method is based on the assumption that η_i and α_i do not depend on the laser length. Our paper investigates the accuracy of this assumption and the reliability of the method.

Both α_i and η_i depend on the carrier density within the quantum wells (QW's). Absorption of photons in long-wavelength lasers is mainly caused by free carriers (intraband transitions) and by intervalence band absorption (IVBA). In both cases, the absorption coefficient rises proportionally to the carrier density. IVBA is stronger with longer wavelength. Carrier losses can be caused by lateral spreading of carriers (η_s), carrier escape from the active region (η_e), and by recombination losses within the active layers (η_r). All three loss mechanisms are enhanced at higher carrier density and contribute to the differential internal efficiency $\eta_i = \eta_s \eta_e \eta_r$ [2]. We have recently shown that QW recombination losses (Auger recombination, spontaneous emission, and Shockley–Read–Hall (SRH) recombination) can dominate the differential internal efficiency due to the nonuniform carrier distribution in multiquantum-well (MQW) laser diodes [3]. In InGaAsP–InP long-wavelength MQW lasers, the largest carrier density occurs in the quantum well closest to the p-doped side because electrons travel more easily across the MQW than holes. Long-wavelength lasers are known to suffer from Auger recombination which rises proportionally to the cube of the local carrier density and which is strongest in the p-side QW. As the MQW carrier nonuniformity increases with rising current, Auger recombination rises since its increment in p-side QW's is larger than its decrement in n-side QW's. In addition, the electron overflow into the p-side separate confinement layer (p-SCL) is enhanced by the carrier nonuniformity since the QW closest to the p-SCL exhibits the highest electron density. In other words, the QW quasi-Fermi levels are not pinned in MQW lasers above threshold as they are with a single active layer [4]. Quantum barriers generate a slight split between the quasi-Fermi levels of neighbor quantum wells and this split increases with rising current. The average MQW carrier density also increases with rising current due to the nonlinear gain vs. carrier density relation [3].

From above considerations, it is obvious that η_i and α_i cannot remain perfectly constant with changing laser length. The modal gain at laser threshold is equal to internal optical loss α_i plus mirror loss α_m. The mirror loss coefficient α_m

rises with shorter cavity length requiring higher MQW gain, i.e., higher MQW carrier density. The higher carrier density causes the internal absorption to increase and the differential internal efficiency to decrease. However, those changes are hard to determine experimentally. Previous loss analysis of red double-quantum well GaInP–GaAs lasers [4] is based on an analytical rate equation model and it relates the dependence $\eta_i(L)$ to vertical leakage assuming length-independent internal optical loss and $\eta_r = 1$. With larger number of quantum wells, numerical models are required to include carrier nonuniformity $(\eta_r < 1)$. We therefore employ an advanced laser simulation software to self-consistently reproduce and study our experimental results. Section II summarizes the numerical laser model. Section III describes the 1.55-μm InGaAsP–InP MQW ridge-waveguide lasers used and the results of measurements with different laser lengths. Section IV analyzes and discusses the loss mechanisms in our lasers and the effect of cavity length variations.

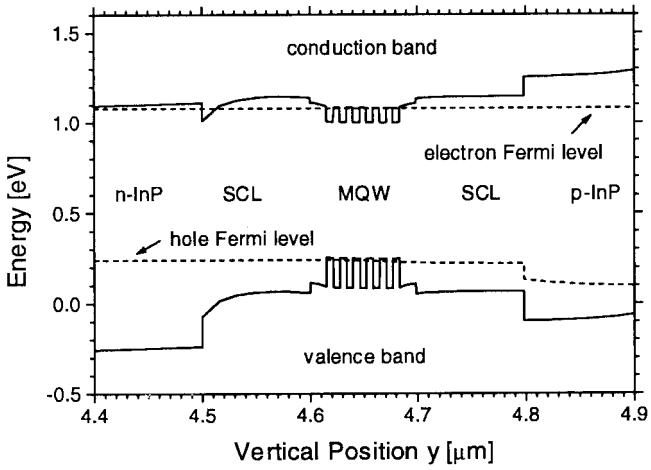

Fig. 1. Active region energy band diagram of our 1.55-μm InGaAsP–InP laser diode.

II. Laser Model and Material Parameters

PICS3D [5], a commercial laser simulation software is used to analyze our measurements and to study internal loss mechanisms. The software self-consistently combines two-dimensional (2-D) carrier transport, wave guiding, and gain calculations with a longitudinal mode solver. Details of the underlying advanced laser models are published in [6] and [7]. We summarize here only those aspects of the models that are most important to the loss analysis. By choosing the highest level of self-consistency, each bias point of our L–I simulation requires about 30 min of computation on a Hewlett-Packard RISC workstation, amounting to 6–10 h for each L–I curve.

The optical gain in our strained quantum wells is computed based on the 4×4 **kp** method [8] including valence band mixing. Band gap shrinkage due to carrier–carrier interaction is considered. The local material gain $g(x, y, z)$ is calculated at every bias point using the local Fermi distribution of carriers within the **kp** bands. Internal optical losses rise linearly with the carrier density [9]. In PICS3D, carrier related absorption is described by $\alpha_c = k_p p + k_n n$ (n: electron density, p: hole density). In 1.55 μm InGaAsP–InP lasers, the absorption due to electrons is very small and we use $k_n = 1 \times 10^{-18}$ cm^2 [9]. Only few direct investigations of the material parameter k_p can be found in the literature on 1.55-μm MQW lasers giving a wide range of $k_p = 20 \cdots 200 \times 10^{-18}$ cm^2 [9]–[12]. Therefore, we use k_p as a fit parameter to find agreement with our L–I measurement. Internal photon losses can also be caused by carrier density independent mechanisms like photon scattering at defects. This is considered by a constant background loss coefficient α_b.

The drift-diffusion model of carrier transport includes Fermi statistics and thermionic emission at heterobarriers [13]. This process is mainly controlled by the offset of conduction band (ΔE_C) and valence band (ΔE_V) at the heterobarrier. We assume a band offset ratio $\Delta E_C/(\Delta E_C + \Delta E_V) = 0.4$ which is typical for the InGaAsP–InP material system [14]. Other important simulation parameters are the SRH recombination lifetime within the QW's ($\tau_n = \tau_p = 2 \times 10^{-8}$ s) and the Auger recombination parameter ($C_n = C_p = 8 \times 10^{-29}$ cm^{-6} s^{-1}). These numbers are in good agreement with the literature on 1.55 μm lasers [15], [16]. The spontaneous recombination rate is obtained self-consistently from the calculated band structure.

III. Device Structure and Experimental Results

The lasers are grown in a metal–organic vapor phase epitaxy horizontal reactor at 645 °C and 350 torr. The active region of the laser structures consists of six 6.4-nm-thick compressively strained (1%) $In_{0.76}Ga_{0.24}As_{0.79}P_{0.21}$ quantum wells. The 5.5-nm-thick barriers are made of lattice matched $In_{0.71}Ga_{0.29}As_{0.55}P_{0.45}$ (1.25-μm bandgap wavelength). The first and the last barrier are 17 nm wide. The MQW stack is sandwiched between 100-nm-thick SCL's of 1.15-μm InGaAsP. On the p-side of the structure, the first 130 nm of InP cladding layer next to the SCL are undoped to prevent diffusion of Zn into the SCL. A highly doped p-InGaAs contact layer is used. Broad area ridge-waveguide lasers with 57-μm-wide stripes are processed. The p-ridge is etched down to the SCL layer. The lasers are characterized as-cleaved. The calculated band diagram of the active region is shown in Fig. 1.

L–I curves are measured under pulsed condition (0.05% duty cycle) to prevent self-heating. L–I measurements are performed with different laser lengths (Fig. 2). Several wire contacts are used with longer lasers to maintain longitudinal homogeneous current injection. However, due to microscopic differences between theoretically identical diodes, the measured L–I curves scatter, especially at larger laser length. These variations are unavoidable and they render the loss analysis more difficult. Fig. 3 plots the inverse slope efficiencies $\eta_d^{-1}(L)$ extracted from the L–I curves. If all data points are taken into account, linear regression (1) delivers a differential internal efficiency of 81% $\pm$ 14% and an internal absorption of 17 cm $\pm$ 6/cm. A facet reflectivity of $R = 0.28$ is assumed. The result is more narrow if we select only the four best lasers with the lowest threshold current and the highest slope efficiency: $\eta_i = 68\% \pm 2\%$ and $\alpha_i =$

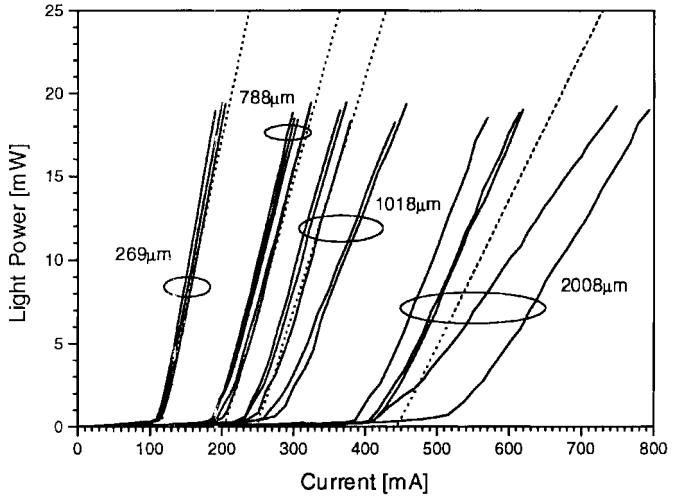

Fig. 2. Measured (solid) and calculated (dotted) L–I characteristics at different laser lengths.

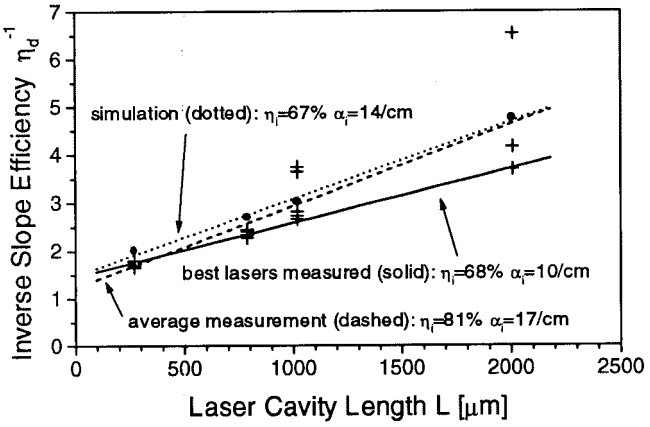

Fig. 3. Inverse slope efficiency $1/\eta_d$ versus laser length L as measured $(+)$ and as calculated $(\bullet)$. Linear regression results are given as lines together with the parameters of (1).

10/cm $\pm$ 1/cm. However, the reliability of this $\eta_d^{-1}(L)$ method is questionable for theoretical and experimental reasons: a) the neglection of cavity length effects on both loss parameters and b) the scattering of experimental data due to microstructural variations and different MQW current injection profiles. We will mainly address the intrinsic accuracy a) in the following.

IV. Numerical Analysis of Experimental Results

The L–I simulation mainly depends on several key material parameters which have to be adjusted carefully to find agreement with the measurement. The Auger coefficient has the strongest impact on the threshold current $I_{\rm th}$ and the optical losses govern the slope efficiency η_d. A higher Auger coefficient requires lower optical losses to obtain the same threshold current, thereby increasing the slope efficiency. The shortest laser fabricated ($L = 269$ μm) is used to find the correct balance between Auger coefficient ($C_n = C_p = 8\times10^{-29}$ cm^{-6} s^{-1}) and total optical losses $\alpha_i+\alpha_m = 67$/cm. The contributions from different optical loss mechanisms are then adjusted to fit measured L–I curves for larger cavity

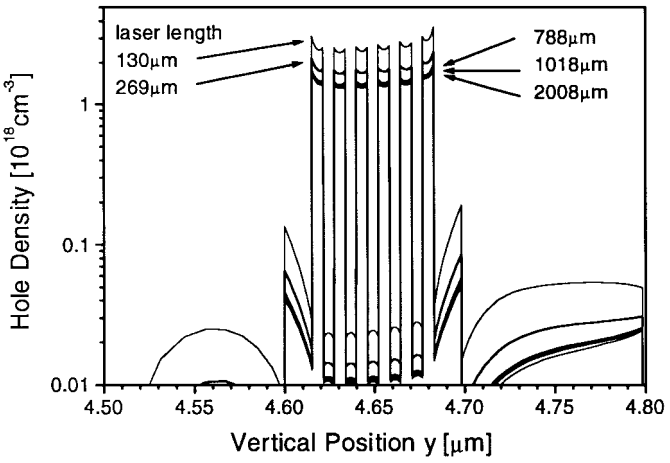

Fig. 4. Calculated hole density profile in the active region at threshold with the laser length L as parameter.

lengths. This results in the hole absorption parameter $k_p = 150 \times 10^{-18}$ cm^2, the background loss parameter $\alpha_b = 0$, and the average facet reflectance $R = 0.28$. Within reasonable limits, this set of optical parameters gives the strongest possible length dependence of optical losses. A weaker length dependence (larger α_b, larger R, smaller k_p) results in a stronger increase of $I_{\rm th}(L)$ and it would give less agreement with the measurement. For each cavity length, we expected the calculated L–I curves to be close to the measured curves of the best lasers (lowest threshold current) which promise almost ideal performance. Instead, the simulated L–I curves are close to the average of measured L–I curves, especially with long lasers. This indicates microscopic differences between the best lasers, e.g., different facet reflectivity. However, we can conclude that carrier density dependent absorption dominates our internal optical losses. Our present investigation is not able to distinguish between different carrier density dependent absorption mechanisms. IVBA is usually assumed to dominate in 1.55 μm lasers and our parameter k_p is near the upper limit of reported IVBA parameters [9]–[12]. Compressive QW strain is often expected to reduce IVBA [10], [11] but recent calculations suggest the opposite [12].

We now employ the same $\eta_d^{-1}(L)$ method as above to compare our simulation to the experimental loss parameters (Fig. 3). The simulation yields the parameters $\eta_i = 67\%$ and $\alpha_i = 14$/cm which are quite close to the measured numbers. However, the theoretical results do not form a perfectly straight line in Fig. 3 indicating length effects on the loss parameters. The remainder of our paper evaluates the intrinsic accuracy of the $\eta_d^{-1}(L)$ method theoretically, extracting the actual functions $\eta_i(L)$ and $\alpha_i(L)$ from our simulations with laser lengths from 130 to 3000 μm.

Fig. 4 plots the vertical hole distribution in the active region at threshold. The QW hole density decreases with larger laser length as well as the hole density in barrier layers and SCL. The strongest drop occurs between short lasers. The mirror loss decrements are smaller with longer lasers and so are the changes in carrier density. From the average QW hole density $p_{\rm QW}(L)$ and the calculated confinement factor of $\Gamma = 0.072$, we obtain the internal loss coefficient $\alpha_i(L) = \Gamma k_p p_{\rm QW}(L)$.

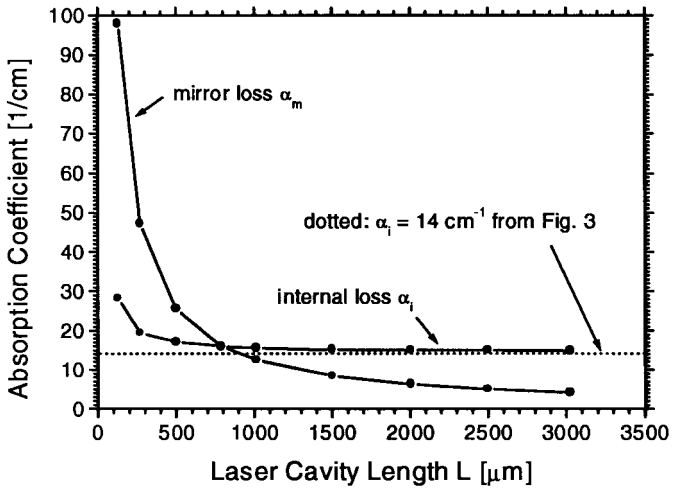

Fig. 5. Optical loss parameters calculated versus laser length.

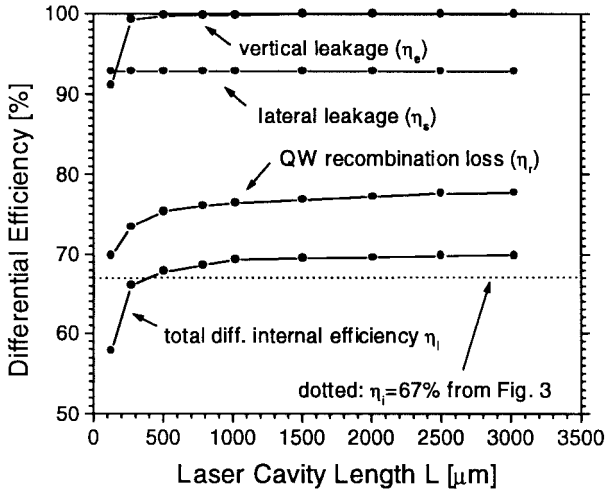

Fig. 6. Differential internal efficiency calculated versus laser length $\eta_i(L)$ and its constituents ($\eta_i = \eta_s \eta_e \eta_r$).

The results are given in Fig. 5. As expected, the internal loss increases with shorter lasers. For comparison, the result of the $\eta_d^{-1}(L)$ method is shown as dotted line and it is only slightly smaller than the actual internal loss in long lasers. The error is less than 10% for $L > 1000$ μm.

The differential internal efficiency $\eta_i = \Delta I_{\rm stim}/\Delta I$ is the fraction of the total current increment ΔI above threshold that results in stimulated emission of photons [17]. We extract this number by three-dimensional (3-D) integration of the stimulated recombination rate at two different bias points above threshold. The first bias point is just above threshold and the second one is near 10-mW lasing power. The calculated function $\eta_i(L)$ is given in Fig. 6. The result $\eta_i = 67\%$ of the $\eta_d^{-1}(L)$ method is only slightly smaller than the actual number of 70% in long lasers. The efficiency $\eta_i(L)$ drops with shorter cavity length and it is below the 10% error margin for $L < 150$ μm ($\eta_i < 60\%$).

Differential carrier losses can be caused by vertical carrier escape from the active layers (current increment ΔI_e), lateral carrier spreading (current increment ΔI_s), and by recombination losses inside the active layers (current increment ΔI_r)

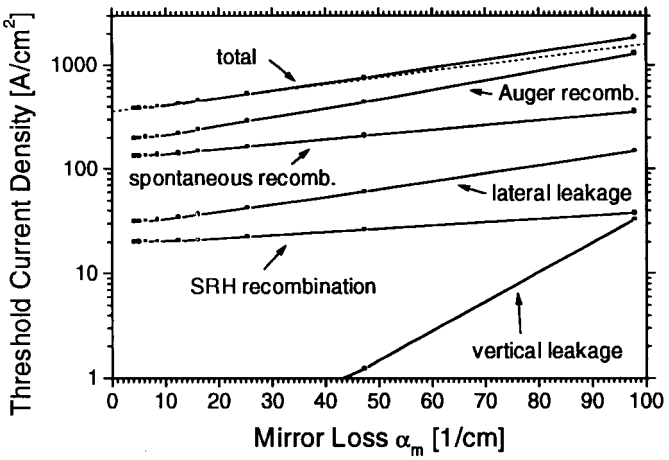

Fig. 7. Calculated threshold current density versus mirror loss $j_{\rm th}(\alpha_m)$ and its constituents (the dotted line is straight, slight data scatter is caused by the numerical integration).

[2]. The total current increment ΔI is the sum of all these contributions

$$\Delta I = \Delta I_{\rm stim} + \Delta I_r + \Delta I_e + \Delta I_s. \tag{2}$$

The corresponding efficiencies are given as

$$\begin{aligned}\eta_i &= \eta_s \times \eta_e \times \eta_r \\ &= \frac{\Delta I_{\rm stim} + \Delta I_r + \Delta I_e}{\Delta I_{\rm stim} + \Delta I_r + \Delta I_e + \Delta I_s} \\ &\quad \times \frac{\Delta I_{\rm stim} + \Delta I_r}{\Delta I_{\rm stim} + \Delta I_r + \Delta I_e} \times \frac{\Delta I_{\rm stim}}{\Delta I_{\rm stim} + \Delta I_r}.\end{aligned} \tag{3}$$

Vertical leakage of electrons (η_e) from the p-SCL can be identified as minority carrier current in the p-InP cladding layer. We obtain a differential efficiency $\eta_e > 99\%$ at all laser lengths except for the shortest laser (Fig. 6). Thus, electron escape at room temperature is only relevant at very high QW carrier densities. The calculated lateral leakage ($\eta_s = 93\%$) is mainly caused by quantum well carriers which leave the active region by lateral diffusion. However, carrier leakage does not dominate the differential internal efficiency of our lasers. The third carrier loss mechanism is the increase in QW recombination losses above threshold. We evaluate these losses by 3-D integration of Auger recombination rate, spontaneous emission rate, and SRH recombination rate at the same two bias points as in the other cases. The computed efficiency $\eta_r(L)$ is given in Fig. 6 and it shows that recombination losses are the strongest contribution to the total carrier loss. Auger recombination is the dominant carrier loss mechanism at room temperature and the nonuniform MQW carrier distribution (Fig. 4) has a stronger effect on η_r at high carrier densities, i.e., at short cavity lengths. The assumption of QW Fermi level pinning above threshold would lead to $\eta_r = 1$ [4].

The threshold current density $j_{\rm th}$ changes exponentially with the optical loss $\alpha_i + \alpha_m$ [17]. Fig. 7 shows the calculated threshold currents versus the mirror loss $\alpha_m = L^{-1}\ln(R^{-1})$. In this logarithmic plot, $j_{\rm th}(\alpha_m)$ deviates slightly from a straight line (dotted) at short cavities which is mainly due to changes of $\alpha_i(L)$. Fig. 7 also shows the contribution of carrier loss mechanisms to the calculated threshold current

density. Auger recombination accounts for more than 50% of the threshold current, spontaneous recombination for about 30%, lateral leakage for about 8%, and SRH recombination for about 3%. Vertical leakage is only noticeable at high carrier densities ($L = 130$ μm).

V. Summary

We investigate the internal optical loss α_i and the differential internal efficiency η_i of 1.55 μm InGaAsP–InP lasers with six quantum wells at room temperature. Both loss parameters are commonly extracted from measurements plotting the inverse slope efficiency versus cavity length $\eta_d^{-1}(L)$. This method neglects the dependence of both the parameters on the cavity length L. We extract the actual functions $\alpha_i(L)$ and $\eta_i(L)$ for our lasers which show that the $\eta_d^{-1}(L)$ method underestimates α_i by more than 10% for $L < 1$ mm. The parameter η_i is within the 10% error margin for $L > 150$ μm. The main contribution to the length dependence of α_i originates in photon absorption by holes. The dependence $\eta_i(L)$ is dominated by quantum well recombination losses which are mainly due to enhanced Auger recombination with increasing MQW carrier nonuniformity.

References

[1] H. Kressel and J. K. Butler, *Semiconductor Lasers and Heterojunction LEDs*. New York: Academic, 1977.

[2] P. M. Smowton and P. Blood, "The differential efficiency of quantum well lasers," *IEEE J. Select. Topics Quantum Electron.*, vol. 3, pp. 491–498, 1997.

[3] J. Piprek, P. Abraham, and J. E. Bowers, "Carrier nonuniformity effects on the internal efficiency of multi-quantum-well lasers," *Appl. Phys. Lett.*, vol. 74, pp. 489–491, 1999.

[4] P. M. Smowton and P. Blood, "On the determination of internal optical mode loss of semiconductor lasers," *Appl. Phys. Lett.*, vol. 70, pp. 2365–2367, 1997.

[5] PICS3D 4.1.2 by Crosslight Software, Inc., 1998.

[6] Z.-M. Li, "Physical models and numerical simulation of modern semiconductor lasers," *Proc. SPIE*, vol. 2994, pp. 698–708, 1997.

[7] PICS3D user manual. [Online]. Available HTTP: http://www.crosslight.ca.

[8] S. L. Chuang, "Efficient band structure calculations of strained quantum wells," *Phys. Rev. B*, vol. 43, pp. 9649–9661, 1991.

[9] Y. Suematsu and A. R. Adams, *Handbook of Semiconductor Lasers and Photonic Integrated Circuits*. London, U.K.: Chapman & Hall, 1994.

[10] I. Joindot and J. L. Beylat, "Intervalence band absorption coefficient measurements in bulk layer, strained and unstrained multiquantum well 1.55 μm semiconductor lasers," *Electron. Lett.*, vol. 29, pp. 604–606, 1993.

[11] G. Fuchs, J. Hoerer, A. Hangleiter, V. Haerle, F. Scholz, R. W. Glew, and L. Goldstein, "Intervalence band absorption in strained and unstrained InGaAs multiple quantum well structures," *Appl. Phys. Lett.*, vol. 60, pp. 231–233, 1992.

[12] T. Cho, H. Kim, Y. Kwon, and S. Hong, "Theoretical study on intervalence band absorption in InP-based quantum-well laser structures," *Appl. Phys. Lett.*, vol. 68, pp. 2183–2185, 1996.

[13] S. M. Sze, *Physics of Semiconductor Devices*. New York: Wiley, 1981.

[14] S. L. Chuang, *Physics of Optoelectronic Devices*. New York: Wiley, 1995.

[15] J. Piprek, D. Babic, and J. E. Bowers, "Simulation and analysis of double-fused 1.55 μm vertical-cavity lasers," *J. Appl. Phys.*, vol. 81, pp. 3382–3390, 1997.

[16] G. P. Agrawal and N. K. Dutta, *Semiconductor Lasers*. New York: van Nostrand Reinhold, 1993.

[17] L. A. Coldren and S. W. Corzine, *Diode Lasers and Photonic Integrated Circuits*. New York: Wiley, 1995.

Joachim Piprek (SM'98) received the Ph.D. degree in solid state physics from Humboldt University, Berlin, Germany, in 1986.

He worked in industry and academia on design and analysis of optoelectronic devices, He is currently an Adjunct Associate Professor at the University of California at Santa Barbara. His research interests include vertical-cavity lasers, novel semiconductor materials, and advanced computer simulation.

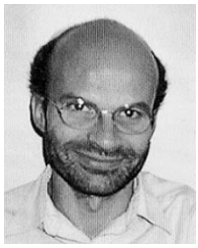

Patrick Abraham received the M.S. and Ph.D. degrees in material science from the University C. Bernard Lyon 1, France, in 1984 and 1987, respectively.

He was a researcher at the Centre National de la Recherche Scientifique (CNRS) and worked until 1988 for the Laboratoire de Physico-Chimie Minérale, France. He is currently a Research Engineer at the University of California at Santa Barbara, where his research interests include laser active region design, MOCVD growth, compliant substrates, and wafer fusing.

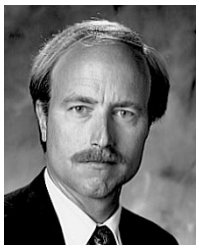

John E. Bowers (S'78–M'81–SM'85–F'93) received the M.S. and Ph.D. degrees in applied physics from Stanford University, Stanford, CA.

He is the Director of the Multidisciplinary Optical Switching Technology Center (MOST) and a Professor in the Department of Electrical Engineering, University of California, Santa Barbara. He is a member of the Optoelectronics Technology Center and the NSF Science and Technology Center on Quantized Electronic Structures. His research interests are primarily concerned with high-frequency optoelectronic devices and physics. He has worked for AT&T Bell Laboratories and Honeywell before joining UCSB. He has published five book chapters, over 200 journal papers, over 200 conference papers, and has received 12 patents.

Dr. Bowers is a Fellow of the American Physical Society, a recipient of the IEEE LEOS William Streifer Award, and is Vice President for Conferences of IEEE LEOS. He is a recipient of Sigma Xi's Thomas F. Andrew prize and the NSF Presidential Young Investigator Award and NSF Graduate Fellowship.